ELECTROMAGNETIC INDUCTION RESEARCH ISSUES: MAGNETIC DIPOLE AND SQUID TECHNOLOGIES

Christopher T. Allen and Najib A. Rehoie

Radar Systems and Remote Sensing Laboratory
Department of Electrical Engineering and Computer Science, University of Kansas
2291 Irving Hill Road, Lawrence, Kansas 66045-2969
TEL: 913/864-4835 * FAX: 913/864-7789 * E-MAIL: graham@ardneh.rsl.ukans.edu

RSL Technical Report 11740-1

September 1995

Sponsored by:

Sandia National Laboratories
Albuquerque NM 87185

AP-4947

Table of Contents

1.0 Introduction 1

2.0 Magnetic Dipoles 2

2.1 Principles 2

2.2 Equivalent Circuit 4

2.3 Frequency Response 4

2.4 Noise 5

2.5 Interference / Shielding Issues 6

2.6 Design Example 6

2.7 State of the Art 7

2.8 Size 8

2.9 Special Requirements / Constraints 8

3.0 SQUIDs 10

3.1 Principles 10

3.2 Equivalent Circuit 12

3.3 Frequency Response 13

3.4 Noise 14

3.5 Interference / Shielding Issues 15

3.6 State of the Art 15

3.7 Size 16

3.8 Special Requirements / Constraints 16

4.0 EMI Evaluation Considerations 17

4.1 Frequencies of Interest / Required Sensitivity 17

4.2 Example: LBL EMI Experiment [Wilt et al., 1983] 17

5.0 Summary / Conclusions 19

6.0 List of Symbols 21

7.0 References 22

8.0 Bibliography 23

8.1 Electromagnetic Induction 23

8.2 Airborne Electromagnetic Induction Techniques 24

8.3 Magnetic Dipole Antennas 25

8.4 SQUID Technology 25

1.0 Introduction

Subsurface probing with electromagnetic induction (EMI) techniques involves measurement of a magnetic field associated with eddy currents induced in the target by a time-varying primary magnetic field. The time-varying nature of this primary field is typically either continuous wave sinusoidal or pulse. Both techniques induce a time-varying secondary magnetic field that can be measured by a sensor or transducer sensitive to time-varying magnetic fields. Several sensor technologies exist for sensing time-varying magnetic fields (e.g., magnetic dipoles [simple wire coils], Hall effect sensors, superconducting quantum interference devices [SQUIDs], and optically pumped magnetometers).

For EMI applications, the *best* technologies are the magnetic dipoles and SQUIDs, based on their relative sensitivity, directionality, cost, size. In this report we will present the underlying operating principles for these two technologies, the current state of the art, and specific characteristics relevant to EMI work (e.g., noise, size, cost).

Regardless of the technology used to measure this secondary magnetic field, a variety of background noise sources will affect this measurement. There are several types of noise sources: micropulsations in the geomagnetic field, lightning (both local and global), noise from electrical power distribution systems, and RF broadcast signals [Burrows, 1978; Keller and Frischknecht, 1966]. The dominant noise source varies with frequency. Below 1 Hz, the micropulsations in the geomagnetic field are the dominant source of noise. Characteristic variations with periods measured in tens of seconds are common. More rapid variations (periods on the order of 0.5 to 2 seconds) are associated with magnetic storms on the sun's surface and auroral displays. For frequencies ranging from around 1 Hz to around 10 kHz, lightning is the dominant noise source. Lightning, which is both sporadic and impulsive in nature, causes local and global variation in the current distribution in the Earth. The spectral content of the noise due to lightning varies with distance from the source; different propagation modes dominate depending on the distance. This coupled with the increased number of electrical storms in progress at greater distances, weights the expected spectra due to lightning such that the energy is found primarily between 1 Hz and 10 kHz. Induction fields about electrical power distribution systems contribute noise at the fundamental frequency (50 or 60 Hz) and at harmonics. Radio frequency broadcasting contributes varying levels of noise across the communications spectrum. Signals in the lower frequency bands, below about 1 MHz, couple into the Earth's surface and propagate via ground or surface waves, resulting in more significant noise levels at distant receivers than those at the higher frequency bands. In fact, geophysicists have explored the use of RF broadcast energy as an energy source in characterizing subsurface properties [Keller and Frischknecht, 1966].

2.0 Magnetic Dipoles

2.1 Principles

A simple loop antenna wound on a ferromagnetic rod is known as an induction magnetometer or magnetic dipole and relies on Faraday's law that states an electromotive force (e.m.f.) is induced in a loop of wire if the magnetic flux through the loop changes. The advantage of using a high-permeability rod is that signal sensitivity is enhanced directly by K_m, the small-signal relative permeability of the rod material, which can be as large as 100,000. For a magnetic intensity H, parallel to the loop axis, varying sinusoidally at frequency f, the induced e.m.f. is given by

$$e.m.f. = \omega n A \mu_o K_e H \tag{2.1}$$

where μ_o is the magnetic permeability of free space ($4\pi \times 10^{-7}$ H/m), K_e is the effective magnetic permeability of the ferromagnetic rod normalized to that of free space, A is the average turns area of the coil, n is the total number of turns, and $\omega = 2\pi f$. This relationship is valid for the ideal case of negligible coil resistance, inductance and capacitance. Note that under these assumptions, the e.m.f. developed is proportional to the oscillation frequency of the magnetic field.

The effective relative permeability, K_e, may be less than the true relative permeability, K_m, due to core demagnetization [Burrows, 1978; Keller and Frischknecht, 1966; Bozorth, 1978]. The effective permeability, K_e, and the true permeability of the material, K_m, are related as

$$\frac{1}{K_e} = \frac{1}{K_m} + \frac{N}{4\pi} \tag{2.2}$$

where $N/4\pi$ is the demagnetizing factor that depends on the ratio length/diameter of the rod [Bozorth, 1978]. A core in the shape of a prolate ellipsoid (major axis length l, two equal minor axes length d) is superior to a cylindrically shaped core as it uses the core material most efficiently by developing a uniform flux density. For a prolate spheroid the demagnetization factor is related to m = l/d, the length to diameter ratio by

$$\frac{N}{4\pi} = \frac{1}{m^2-1}\left\{\frac{m}{\sqrt{m^2-1}}\ln\left(m+\sqrt{m^2-1}\right)-1\right\} \tag{2.3}$$

Table 2.1 lists demagnetization factors for rods and prolate ellipsoids.

TABLE 2.1. DEMAGNETIZATION FACTORS, $N/4\pi$, FOR RODS AND PROLATE ELLIPSOIDS MAGNETIZED PARALLEL TO THE LONG AXIS. [Bozorth, 1978]

Dimension Ratio (length/diameter)	Rod	Prolate Ellipsoid
0	1.0	1.0
1	0.27	0.3333
2	0.14	0.1735
5	0.040	0.0558
10	0.0172	0.0203
20	0.00617	0.00675
50	0.00129	0.00144
100	0.00036	0.000430
200	0.000090	0.000125
500	0.000014	0.0000236
1000	0.0000036	0.0000066
2000	0.0000009	0.0000019

As an example, consider a cylindrical rod with a variety of dimension (length to diameter) ratios and true relative permeabilities. Table 2.2 lists the effective permeability (K_e) for these cases. Note that for dimension ratios less than around 20, the effective relative permeability is geometry limited (i.e., the effective permeability is relatively insensitive to the actual permeability), whereas for dimension ratios above about 500, the effective permeability is permeability limited.

TABLE 2.2. EFFECTIVE RELATIVE PERMEABILITY FOR A ROD FOR A VARIETY OF DIMENSION RATIOS AND TRUE RELATIVE PERMEABILITIES

Dimension	True Relative Permeability					
Ratio	**50**	**100**	**500**	**1000**	**5000**	**10000**
0	0.98	0.99	1.00	1.00	1.00	1.00
1	3.45	3.57	3.68	3.69	3.70	3.70
2	6.25	6.67	7.04	7.09	7.13	7.14
5	16.67	20.00	23.81	24.39	24.88	24.94
10	26.88	36.76	52.08	54.95	57.47	57.80
20	38.21	61.84	122.40	139.47	156.99	159.49
50	46.97	88.57	303.95	436.68	671.14	719.42
100	49.12	96.53	423.73	735.29	1785.71	2173.91
200	49.78	99.11	478.47	917.43	3448.28	5263.16
500	49.97	99.86	496.52	986.19	4672.90	8771.93
1000	49.99	99.96	499.10	996.41	4911.59	9652.51
2000	50.00	99.99	499.78	999.10	4977.60	9910.80

2.2 Equivalent Circuit

The equivalent circuit for a typical magnetic dipole is composed of a large resistance, an appreciable inductance and capacitance between the windings [Keller and Frischknecht, 1966]. In general, the magnetic core losses can be minimized by using a core composed of thin laminations of ferromagnetic material as is done in transformer manufacture. An equivalent circuit is shown in Figure 2.1.

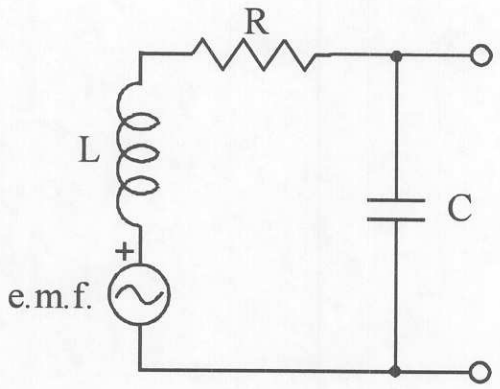

Fig. 2.1. Equivalent circuit for an induction coil used for measuring the rate of change of a magnetic field [Keller and Frischknecht, 1966].

The internal resistance of the coil, R, is given by [Burrows, 1978]

$$R = \frac{2\pi a n^2}{\sigma_c C_w A_c} \tag{2.4}$$

where a is the average turn radius, n is the total number of turns, σ_c is the conductivity of the wire conductor, A_c is the cross-sectional area available for the winding and C_w is the filling factor. C_w is less than unity and the ratio of total conductor cross section to winding area (i.e., $C_w = A_c/nA_w$ where A_w is the cross-sectional area of a single wire).

In addition to the internal, ohmic resistance, external resistance must also be considered. The radiation resistance of the dipole in air is negligible compared with its internal resistance, R. In many applications the dipole will be in close proximity (relative to a wavelength) to the Earth or other conducting media and the mutual resistance will be greater than the radiation resistance. However, even in cases where the coil is buried in natural Earth media, the internal resistance will exceed these external resistance components [Burrows, 1978].

2.3 Frequency Response

The maximum voltage output will occur at the resonant frequency [Keller and Frischknecht, 1966]

$$\omega_R = \sqrt{\frac{1+R/R_{in}}{LC}} \tag{2.5}$$

where R_{in} is the input resistance of the receiver that connects to the sensor. At this resonant frequency, the output voltage may exceed that given in (2.1) depending on the load and the parameters of the coil. At about 10% of ω_R, the output voltage will be nearly that predicted by (2.1). For frequencies above ω_R the output voltage will decrease with increasing frequency. Thus, the induction coil is a relatively narrow band sensor.

Changing the parameters of the coil alters its performance [Keller and Frischknecht, 1966]. Increasing the number of turns in the coil, n, does not appreciably increase the output voltage; however, what occurs is a proportionate reduction in the resonant frequency. Increasing the product of core-effective permeability and cross-sectional area, K_eA, does increase the output voltage at all frequencies but also reduces the resonant frequency.

The dipole can also be characterized in terms of its Q or quality factor. For the circuit shown in Fig. 2.1, the Q is given by

$$Q = \frac{\omega_R L}{R} \tag{2.6}$$

The Q also relates the bandwidth to the resonant frequency where the bandwidth is defined as the range of frequencies over which the output voltage is larger than $1/\sqrt{2}$ times its maximum value.

$$Q = \frac{\omega_R}{BW} \tag{2.7}$$

High Q systems therefore have a relatively narrow band frequency response whereas low Q systems have a wider band of frequency response.

The resonant frequency can be changed through the addition of external tuning elements (i.e., capacitors and inductors). Similarly, the Q of the circuit can be reduced through the addition of external resistance.

2.4 Noise

A variety of noise sources affect the magnetic field measurement. Those unique to the magnetic dipole are magnetostrictive noise and thermal noise.

Magnetostrictive noise is produced when a mechanical stress or strain is applied to the ferromagnetic core material with a bias flux density in it. Under these conditions the mechanical forces on the core will cause the bias flux density to change. Techniques for reducing this noise source include canceling the geomagnetic flux bias through a demagnetizing

winding, selecting a core material with a low magnetostrictive sensitivity, and using a stress-relieving core construction [Burrows, 1978].

Thermal noise arises from the ohmic losses in the wire coil. The open-circuit, thermal-noise voltage spectral density $S_v(\omega)$ is [Burrows, 1978]

$$S_v(\omega) = \sqrt{4kTR} \tag{2.8}$$

in $V/\sqrt{Hz}$ where k is Boltzmann's constant (1.38×10^{-23} J/K) and T is the physical temperature of the coil in Kelvins. This noise voltage can be expressed as an equivalent magnetic field noise and is given by

$$S_h(\omega) = \frac{\sqrt{4kTR}}{\omega n A \mu_o K_e} \tag{2.9}$$

in $A/m/\sqrt{Hz}$. Using (2.4) we get

$$S_h(\omega) = \frac{2}{A\omega\mu_o K_e}\sqrt{\frac{2\pi kTa}{\sigma_c C_w A_c}} \tag{2.10}$$

where A_c is the available winding cross-sectional area. Note that in (2.10) the number of turns, n, does not appear. Thus, for a magnetic dipole, the thermal noise is independent of the number of turns in the coil.

2.5 Interference / Shielding Issues

Electrostatic shielding of the dipole may be advantageous. The application of a grounded, conformal metallic coating or other metal housing will generally suffice. Care must be taken to ensure that an electrical break in the shield occurs at some point around the circumference of the coil to avoid a short-circuited turn the shield would otherwise represent [Burrows, 1978]. Also, adequate spacing between the shield material and the coil may be necessary to avoid increasing the stray capacitance of the assembly, which would result in a lower self-resonant frequency.

2.6 Design Example

Consider a dipole antenna with the following properties (see Table 2.3) used to sense a magnetic intensity of 10^{-10} A/m at a frequency of 100 kHz.

TABLE 2.3. MAGNETIC DIPOLE DESIGN EXAMPLE PARAMETERS

Parameter	Value
Core Shape	cylinder
Core Length	12 inches (~30.5 cm)
Core Diameter	1 inch (~2.5 cm)
K_m of Core Material	6000
Number of turns	500

For a cylindrical rod with a length/diameter ratio of 12 the demagnetization factor is, by interpolating data from Table 2.1, $N/4\pi = 0.015$.

From (2.2) the effective relative permeability is found to be $K_e = 66$.

Assuming the average-turns area of the coil is the cross-sectional area of the core, we get $A = 5 \times 10^{-4}$ m^2 and from (2.1) the e.m.f. developed in the coil is approximately 1 nV.

Assuming a solenoidal coil is fabricated from copper wire ($\sigma_c = 5.8 \times 10^7$ S/m) with a conductor diameter of 10 mils (0.01 inch or 0.25 mm) and a total diameter of 11 mils with the insulating dielectric coating, a filling factor of 65 % ($C_w = 0.65$), and a cross-sectional area available for the winding (A_c) of 0.39 m^2, we find using (2.4) that $R = 1.4$ mΩ.

Using this value for the internal resistance, and assuming it to be at room temperature (290 K), the open-circuit, thermal-noise voltage spectral density ($S_v(\omega)$) is found to be 4.7 pV/$\sqrt{\text{Hz}}$ and the equivalent magnetic field noise ($S_h(\omega)$) is 3.5×10^{-13} A/m/$\sqrt{\text{Hz}}$.

Capacitance and inductance would be determined experimentally to determine the resonant frequency and the Q of the dipole.

2.7 State of the Art

The magnetic dipole used by RTR Inc. (Stolarczyk, 1995) has been described to have the characteristics listed in Table 2.4. These parameters are consistent with the parameters used in the preceding design example (Section 2.6). The stated sensitivity of 0.3 fT/$\sqrt{\text{Hz}}$ at a center frequency of 100 kHz is comparable to that of SQUID devices discussed later.

This dipole is connected to the EMI receiver as shown in Fig. 2.2. The capacitor, C, immediately following the dipole (inside the box) serves to tune the circuit to a desired center frequency. The impedance matching transformer and attenuator arrangement serve to set the Q (BW) of the circuit. The remainder of the diagram illustrates the down-conversion and synchronous detection of the received signal. As shown, the transmitter and receiver share a common oscillator providing a stable phase reference.

TABLE 2.4. RTR'S MAGNETIC DIPOLE CHARACTERISTICS [STOLARCZYK, 1995]

Parameter	Value
Length	12 inches
Diameter	1 inch
K_m	6000
Q (unloaded)	200-300
e_n (BW of 1 Hz)	0.6 $nV/\sqrt{Hz}$
Sensitivity @ 100 kHz	0.3 $fT/\sqrt{Hz}$
e.m.f. @ $H = 10^{-10}$ A/m	1 nV

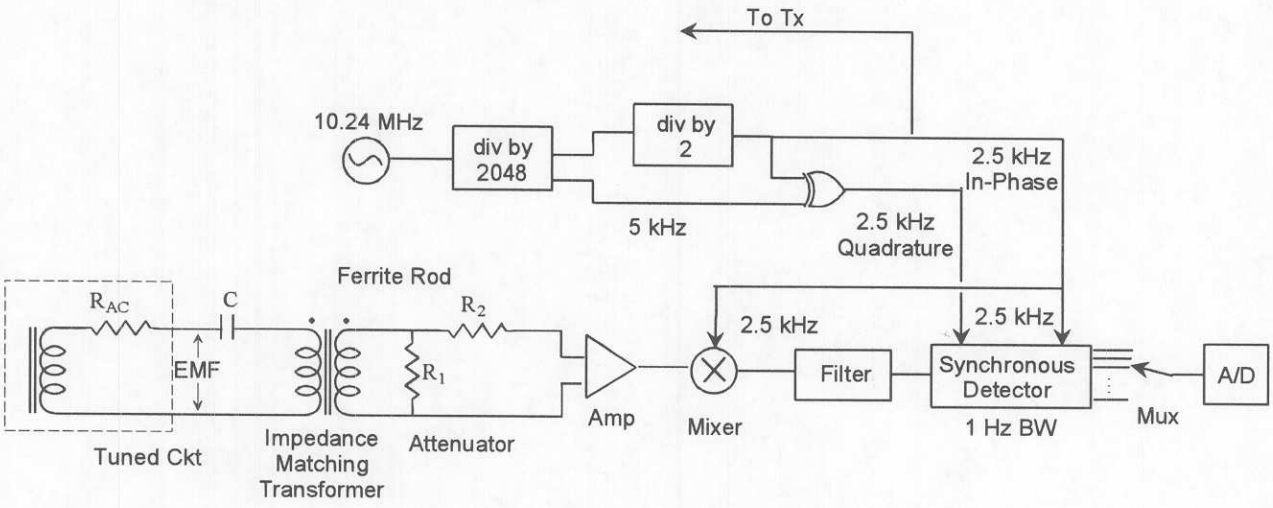

FIG. 2.2. EMI receiver circuit implemented by RTR Inc., [Stolarczyk, 1995].

2.8 Size

The size of magnetic dipoles, as discussed previously, is directly related to the sensor sensitivity. Efforts to miniaturize the magnetic dipole through scaling must result in decreased sensitivity. Currently reported dipole sizes exceed 30 cm in the greatest dimension.

2.9 Special Requirements / Constraints

While the primary advantage of using a magnetic dipole with a ferromagnetic core is to increase sensitivity, there are disadvantages. Burrows [1978] lists three disadvantages associated with ferromagnetic-core magnetic dipoles: (i) the permeability of magnetically soft materials used for the core cannot be determined accurately in advance; (ii) the magnetic material is mechanically soft and very sensitive to mechanical strain and temperature; (iii) dipole coupling to the geomagnetic field, which may be sufficient to saturate the core material,

will reduce the small-signal permeability and, hence, the sensitivity. The effects described in (i) and (ii) can be reduced by designing the dipole such that the effective permeability is geometry limited rather than permeability limited. One possible solution to the problem of saturation by the geomagnetic field is to introduce a degaussing winding carrying a very-low-noise DC current, effectively canceling the axial component of the geomagnetic field within the core.

Keller and Frischknecht [1966] discuss the sensitivity to coil movement, translational or rotational, which may change the coupling with the geomagnetic or other local magnetic fields. This issue is not, however, unique to magnetic dipoles. Any magnetic sensor with significant directivity will be similarly affected by such movement. Two solutions to this particular disadvantage have been proposed. The first involves using three magnetic sensors arranged in an orthogonal pattern such that the total flux detected by this array is independent of orientation. The sensor orientation relative to a time-invariant magnetic field could then be obtained via signal processing and this effect removed. The second approach is to form a differential gradiometer wherein the difference is taken of outputs from multiple sensors that are mechanically aligned. This concept is described in more detail in the discussion on SQUIDs.

One other disadvantage of magnetic dipole sensors is related to their size. From (2.1) it is clear that the sensitivity is directly proportional to the average turns area of the coil, A, which is usually the same as the cross-sectional area of the core, A_f. We know from the previous discussion that it is desirable to have the rod length much greater than the rod diameter. Therefore to improve sensitivity, a dipole using a long rod is required. In many applications this may be acceptable; however in borehole applications this is not the case. For boreholes of reasonable diameters, geometrical and mechanical constraints will limit the dipole sensitivity to magnetic fields parallel to the borehole axis.

3.0 SQUIDs

3.1 Principles

Superconducting quantum interference devices (SQUIDs), the most sensitive detectors of magnetic flux available, are flux-to-voltage transducers, providing an output voltage that is periodic in the applied flux with a period of one flux quantum,

$$\Phi_o \equiv \frac{h}{2q} \approx 2.07 \times 10^{-15} \text{ Wb} \tag{3.1}$$

where h is Planck's constant (6.6256×10^{-34} J s) and q is the electronic charge (1.60218×10^{-19} C) [Clarke, 1989]. This flux quantum is extremely small — it is roughly the amount of magnetic flux intercepted by a red blood corpuscle (about 7 μm in diameter) in the Earth's magnetic field (50 μT) [Clarke, 1994]. [Note: 1 Wb/m^2 = 1 T.] Three physical phenomena (superconductivity, flux quantization and Josephson tunneling) are combined in the SQUID. Superconductivity refers to the resistanceless flow of electric current at cryogenic temperatures, which requires dewars and cryogenic liquids to maintain temperatures to support superconductive behavior. Flux quantization refers to the fact that the flux in a closed superconducting loop is quantized in units of Φ_o. Josephson tunneling refers to electrical current flowing through a superconductor-insulator-superconductor junction.

The total magnetic flux (the product of the magnetic field density and the area enclosed by the loop) cannot take on arbitrary values; rather it must equal an integral number of flux quanta, Φ_o. Also, the Josephson junction has a characteristic critical current, I_o (the maximum superconductor current that can flow through the junction), that is dependent on the junction size, the superconducting material and the temperature. The current flowing through the SQUID is affected by an externally applied bias current and the current induced by the external magnetic field. For example, an increase in the magnetic field causes the SQUID current to increase until it reaches the critical current level (maximum), at which time the SQUID current decreases until it reaches a minimum level and then again begins increasing. The SQUID voltage is measured in practice, not the SQUID current. This voltage also swings back and forth between maximum and minimum levels in a steadily changing magnetic field, thus a flux-to-voltage transducer results. However the output voltage is periodic and not single valued. To determine uniquely the magnetic field level or relative changes in this level, feedback electronic circuits (sometimes referred to as lock-in circuits or amplifiers) are used to remove the ambiguities.

There are two kinds of SQUIDs, the DC SQUID and the RF SQUID. The DC SQUID consists of two (or more) Josephson junctions connected in parallel on a superconducting loop

and operates with a steady bias current. The RF SQUID involves a single Josephson junction interrupting current flow in a superconducting loop with an inductively coupled RF bias.

Due to the resistanceless nature of the superconducting coil, it is possible to induce a nondecaying current by introducing a static magnetic field. In addition, SQUIDs are almost always coupled to an input circuit to take advantage of the high sensitivity. For magnetometers, a flux transformer (a loop of superconducting material coupled to a SQUID) is used to boost the field sensitivity by as much as 100 fold or more [Clarke, 1994]. This increase in sensitivity is possible as the pickup loop encloses a much larger area than can the SQUID. The input circuit is composed of a pickup loop connected to the input coil that is magnetically coupled to the SQUID as illustrated in Fig. 3.1.

Magnetic flux gradiometers are obtained when two oppositely wound pickup loops are connected in series with the input coil, as shown in Fig. 3.1. In a homogeneous magnetic field the effects on the two loops cancel and the gradiometer is insensitive. In the presence of a magnetic gradient the cancellation is not complete as the flux in each of the two pickup loops is different. Thus a gradiometer is effective in measuring fields produced by nearby sources, and sensitivity decreases as the separation between the SQUID and source increase. Gradiometers have been developed in a variety of geometries, for example axial and planar. Planar gradiometers, which are more easily implemented in thin-film processes, measure an off-diagonal gradient. Gradiometer sensitivity is dependent on source distance and according to Falco [1978] the present limit on gradient sensitivity is about 100 fT/m.

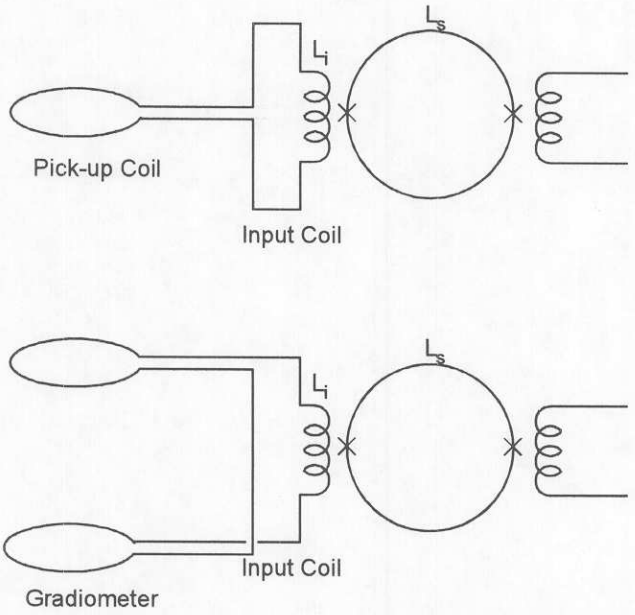

FIG. 3.1 Superconducting flux transformers. Top — Magnetometer. Bottom — First-derivative gradiometer [Clarke, 1989].

3.2 Equivalent Circuit

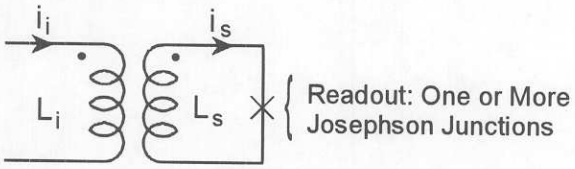

FIG. 3.2 Schematic representation of a SQUID magnetometer and input coil. The readout circuit uses one or more Josephson junctions to monitor the magnetic flux induced in the superconducting SQUID loop [Giffard, 1980].

The equivalent circuit for a SQUID magnetometer is shown in Fig. 3.2. The input coil inductance, L_i, and the SQUID circuit inductance, L_s, are coupled and a current, i_i, in the input coil induces a flux, Φ_{si}, in the SQUID circuit given by

$$\Phi_{si} = i_i \, k_{si} \sqrt{L_i \, L_s} \tag{3.2}$$

where k_{si} is the coefficient of coupling between L_i and L_s [Giffard, 1980]. The Josephson junction(s) — one in RF SQUIDs, two or more in DC SQUIDs — in the SQUID circuit responds to the phase of the superconducting wavefunction and is periodic in the applied flux to the flux quantum, Φ_o. This phase may be expressed in terms of a dimensionless angle, which is the normalized SQUID flux θ_{si},

$$\theta_{si} = 2\pi \frac{\Phi_{si}}{\Phi_o} \tag{3.3}$$

The SQUID current, i_s, and the output voltage, v_r, can be expressed as periodic functions of the applied flux as

$$v_r(\theta_{si}) = v_o \left\{ \frac{a_o}{2} + \sum_{n=1}^{\infty} a_n \cos n\theta_{si} + \sum_{n=1}^{\infty} b_n \sin n\theta_{si} \right\} \tag{3.4}$$

$$i_s(\theta_{si}) = j_o \left\{ \sum_{n=1}^{\infty} c_n \cos n\theta_{si} + \sum_{n=1}^{\infty} d_n \sin n\theta_{si} \right\} \tag{3.5}$$

The shape of the forward transfer function $v_r(\theta_{si})$ can vary from triangular in the case of an ideal RF SQUID to sinusoidal in a well-behaved DC SQUID [Giffard, 1980]. The SQUID current and the output voltage are related through the small-signal, forward transfer ratio, Z_f, as

$$v_r = Z_f \, i_s \tag{3.6}$$

Fig. 3.3 shows an RF SQUID consisting of a superconducting loop of inductance L_s, interrupted by a single Josephson junction. The Josephson junction has a critical current I_o, a

self-capacitance C, and a resistive shunt R. The critical current is chosen so that $L_s I_o \sim \Phi_o$. The loop is inductively coupled with a coupling coefficient, K, to the inductor of the tank circuit that is excited by an RF current at its resonant frequency. The tank circuit is composed of the tank inductor, L_T, a parallel capacitor, C_T, and a parallel resistor, R_T. Optimum performance is obtained when $K^2Q \sim 1$, where Q is the quality factor of the tank circuit. SQUID operation is monitored through the amplitudes of the RF current and the voltage obtained by demodulating the RF signals. At a constant RF bias current, the demodulated voltage is periodic in Φ, with a transfer function

$$V_\Phi \approx \omega_{RF} \sqrt{\frac{Q L_T}{L_s}} \tag{3.7}$$

A modulating flux, typically between 100 and 500 kHz with a peak-to-peak amplitude of $\Phi_o/2$, is also applied to the SQUID, just as in the case of the DC SQUID [Clarke, 1989].

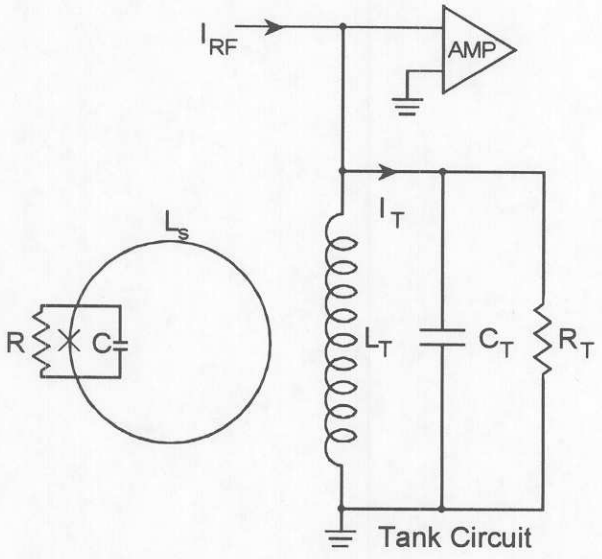

FIG. 3.3 RF SQUID inductively coupled to a resonant tank circuit [Clarke, 1989].

3.3 Frequency Response

The frequency response of the SQUID may extend well into the microwave frequencies and beyond; it is the bandwidth of the interfacing electronics that limits the system bandwidth. DC SQUIDs, which are biased directly with a DC current, are capable of measuring static magnetic flux levels. RF SQUIDs, which are biased through inductively coupled RF energy, require modulated fluxes.

The electronics involved typically include amplifiers, lock-in amplifiers and feedback to create a flux-locked loop. This feedback circuit is used as a null detector of magnetic flux. By applying a modulating flux of an appropriate amplitude to the SQUID, a quasistatic flux is present in the SQUID resulting in a linear output voltage versus applied external magnetic flux.

For DC SQUID applications, reported bandwidths typically extend up to about 500 kHz. For RF SQUID applications, frequencies of 20-30 MHz have been reported [Clarke, 1989].

3.4 Noise

The Josephson junctions in the DC SQUID represent resistive elements and contribute thermal noise in the SQUID. The spectral noise density of the voltage across the SQUID at a fixed bias current is

$$S_v(\omega) \cong 16\,k\,T\,R \tag{3.8}$$

where k is Boltzmann's constant, T is the physical temperature of the SQUID and R is the resistance associated with the Josephson junctions. This voltage noise is related to an equivalent flux noise as

$$S_\Phi(\omega) = \frac{S_v(\omega)}{V_\Phi^2} \tag{3.9}$$

where

$$V_\Phi \equiv \left| \left(\frac{\partial V}{\partial \Phi} \right)_I \right| \tag{3.10}$$

is the transfer coefficient measured at the steepest part of the V-Φ curve. A typical LTS (4.2 K) DC SQUID with an R = 5 Ω results in a noise voltage density ($S_v(\omega)^{1/2}$) of about 70 pV/$\sqrt{\text{Hz}}$ and a flux noise of approximately $10^{-6}\ \Phi_o/\sqrt{\text{Hz}}$ [Clarke, 1989].

Thermal noise in the RF SQUID is characterized by an equivalent intrinsic flux noise spectral density [Clarke, 1989]

$$S_\Phi(\omega) \approx \frac{(L_s I_o)^2}{\omega_{RF}} \left(\frac{2\pi k T}{I_o \Phi_o} \right)^{4/3} \tag{3.11}$$

Unlike the case of DC SQUIDs, extrinsic noise sources will be significant with an RF SQUID. These include cable losses and preamplifier noise. For this reason, special care should be exercised in the design of these circuits.

Both DC and RF SQUIDs suffer from 1/f noise, which arises from electron tunneling in the Josephson junction and the motion of flux lines in the body of the SQUID. This *flicker* noise is significant if frequencies of interest are at 0.1 Hz or less. In general, this 1/f noise is greater for HTS SQUIDs than for LTS SQUIDs.

Clarke [1989] discusses a typical LTS RF SQUID device having white (thermal) noise energy levels of 5 x 10^{-29} J/Hz with a 1/f noise energy of 10^{-28} J/Hz at 0.1 Hz.

3.5 Interference / Shielding Issues

The DC SQUID is the most sensitive magnetometer available. As such, it is susceptible to extraneous signals that may corrupt the measurement of interest. In many applications, measurements are made in magnetically shielded rooms or the SQUID may be housed in a shielded enclosure. As discussed in the introduction, many sources of magnetic noise exist, both naturally occurring and manmade. For measurements made in the field, as would be required for EMI, shielding is not a viable solution. Other solutions, such as gradiometers, are required.

3.6 State of the Art

The fundamental sensitivity and noise performance of the basic SQUID are determined by the quantum physics. Practical implementation introduces additional sources for degradation. As discussed above, the SQUID sensitivity is measured in flux quanta and increased sensitivity is gained through the use of a flux transformer. State-of-the-art systems incorporate several innovations. In RF SQUIDs noise contributions from the tank circuit and the preamplifier are important. Thermal fluctuations will induce noise on the RF voltage across the tank circuit.

The advent of high-temperature superconductors made practical many more SQUID applications. While high-temperature superconductor (HTS) SQUIDs, which use liquid nitrogen (77 K) cooling, cannot achieve the resolution of the low-temperature superconductor (LTS) SQUIDs, which use liquid helium (4.2 K) cooling [Clarke, 1994], the advantages associated with the HTS SQUIDs make them desirable. These advantages include both the relative cost of the cryogenic coolant, the availability of the coolant, and, most important, the consumption rate of the coolant. Liquid nitrogen may be an order of magnitude less expensive than liquid helium and is considerably more readily procured. The greatest advantage in using HTS over LTS is that the latent heat of vaporization of liquid nitrogen is about 60 times that of liquid helium so, while a dewar of liquid helium may require replenishment every few days, the liquid nitrogen may require replenishment only every few weeks.

DC SQUID devices have been developed into low-noise amplifiers for frequencies up to 100 MHz or more [Clarke, 1989]. By integrating such a preamplifier within the same package as the SQUID, the system effective temperature could be significantly reduced as both the intervening cabling and the amplifier itself would be at cryogenic temperatures and the cable length would be minimized.

Conductus, Inc. of San Diego, California, offers commercially available DC SQUIDs with performance comparable to those achieved in research laboratories. For example, an LTS DC

SQUID has an input coil sensitivity of less than 0.2 $\mu\Phi_o/\sqrt{Hz}$ above 1 Hz and a noise level of less than 20 $\mu\Phi_o/\sqrt{Hz}$. Their HTS DC SQUIDs have sensitivities of less than 25 $\mu\Phi_o/\sqrt{Hz}$ above 1 Hz and field noise levels of less than 1 $fT/\sqrt{Hz}$ down to 1 Hz. These sensors are available configured both as magnetometers and as planar gradiometers. System bandwidths are selectable between 5 Hz, 500 Hz, 5 kHz and 50 kHz. The flux-locked loop module interfaces to the controller via fiber-optic cable to minimize RFI effects. They also offer liquid helium and liquid nitrogen dewars to provide operation for about a month. With dimensions of 58 mm x 18 mm x 10 mm for their LTS sensor and 39 mm x 19 mm for their HTS sensor, the sensors can be used in borehole applications [Conductus, 1995].

Los Alamos National Laboratory scientists [Reagor, 1995] are developing HTS DC SQUIDs using semiconductor processing techniques. They report sensitivities of 100 $fT/\sqrt{Hz}$ with bandwidths up to 20 kHz (limited by the external electronics — both commercial and custom built). This device is sensitive to fields ranging from 10^{-6} Φ_o to 500 Φ_o yielding a dynamic range of approximately 87 dB, again limited by the external electronics, in this case a commercial flux-lock loop.

3.7 Size

Size the one of the significant advantages of the SQUID when compared to the magnetic dipole. As mentioned in the section entitled State of the Art, the Conductus HTS DC SQUID comes in a 39-mm x 19-mm package.

3.8 Special Requirements / Constraints

As discussed previously, there are special requirements of the SQUID sensor. The device must be kept in a cryogenic environment. This requires a dewar and temperature-monitoring techniques. Also, the SQUID requires the application of a modulating flux and the use of a flux-locked loop. These requirements are unique to the SQUID sensor.

4.0 EMI Evaluation Considerations

4.1 Frequencies of Interest / Required Sensitivity

One of the advantages of using EMI for subsurface probing is its ability to sense targets at great depths. As penetration depth and frequency are closely related, the usable frequency must be constrained to support the penetration depth of interest. For typical rock/soil conditions, to penetrate to depths exceeding 10 m, the upper limit of the frequencies of interest will generally be in the few MHz to tens of MHz. Substantially deeper probing further constrains this upper frequency limit. As discussed below, in probing to depths of approximately 2 km, a system with a maximum frequency of 500 Hz was used.

In addressing the required SQUID sensitivity for a variety of applications, Clarke [1989] addressed the sensitivity requirements for electromagnetic sounding (EMI) and reported that the level is approximately 10 $fT/\sqrt{Hz}$.

4.2 Example: LBL EMI Experiment [Wilt et al., 1983]

Lawrence Berkeley Laboratory (LBL) conducted electromagnetic induction experiments in 1979 to demonstrate the applicability of this technology in geothermal exploration. The LBL-developed system, the EM-60, is a frequency domain system using three-component magnetic detection. For excitation, a ±65 A square wave current is applied to a four-turn, 100-m horizontal loop over a frequency range of 0.05 to 500 Hz. With transmitter-receiver separations of up to 4 km, exploration depths of 2 km or more were yielded. Using this system, a conductive zone at a depth of 200 m was detected and a nearby drillhole confirmed the presence of 100°C water at that depth. While the use of electromagnetic induction is not new, what is significant about this report is the application of SQUIDs in the receiving magnetometer.

Three-component SQUID magnetometers detected magnetic fields at two receiver sites. These were oriented to measure the vertical, radial, and tangential components with respect to the excitation loop. A hard-wire link between a shunt resistor on the excitation loop and the receiver electronics was used to provide an absolute phase reference; however, this arrangement was found to be a source of noise, particularly at frequencies above 50 Hz. Researchers eliminated the absolute phase reference at high frequencies in favor of relative phase measurements between the vertical and radial measurements. In addition, naturally occurring geomagnetic noise, which follows a 1/f frequency response, posed a formidable barrier to low-frequency measurements. To reduce the effect of this geomagnetic noise, a second SQUID magnetometer was placed at a distance sufficiently far from the excitation loop (about 10 km) to be relatively insensitive to it, and this receiver observed these same geomagnetic fluctuations. These data were then subtracted from the primary receiver data.

This technique was successful in reducing the effect of geomagnetic noise in these EMI measurements.

The Wilt et al. [1983] report documents the utility of SQUID technology in electromagnetic induction field experiments.

5.0 Summary / Conclusions

The magnetic dipole, as described, has been found to be a very sensitive sensor of time-varying magnetic fields. A sensitivity of 0.3 $fT/\sqrt{Hz}$ at 100 kHz is more than adequate for EMI applications. The difficulty deals not with sensitivity but rather with resonant frequency and size. There are other difficulties as well, such as the mechanical properties of the ferromagnetic material, saturation of the core material by the geomagnetic field, and sensitivity to dipole movement. However these problems have technical solutions requiring good engineering to reduce these effects to acceptable levels. The issue of resonant frequency (i.e., operating an EMI system at MHz frequencies) is a more fundamental problem. This resonant frequency is determined by the inductance and capacitance of the dipole winding plus any external capacitance and inductance deliberately introduced. To overcome this limitation, techniques to minimize the capacitance may be studied. However, a more fundamental course may be appropriate. Operating a magnetic dipole outside of its tuned region or flattening the frequency response of the circuit (substantially lowering the Q) introduces a reduction in sensitivity, yet the available sensitivity may be adequate to meet system requirements.

A more fundamental challenge is the size requirement for a magnetic dipole. For free space measurements, the size of currently available dipoles may be acceptable. However, other applications, such as borehole sensing, require a size reduction by about an order of magnitude to detect any fields other than those parallel to the borehole axis. Given the operating principles of the magnetic dipole, a scaled reduction of the ferrite rod necessarily translates into a corresponding reduction in sensitivity. The equivalent magnetic field noise will also be reduced, according to (2.10), when a scaled-down ferrite core is used.

The dynamic range of the magnetic dipole is limited primarily by the receiver electronics. There is of course an inherent dynamic range limitation of the magnetic dipole due to saturation of the core material; however this level is typically well beyond the dynamic range of the receiver electronics.

The main advantages of SQUID magnetometers are low noise (even with compact detection coils), a large dynamic range, a wide frequency band (that starts at DC), the ability to selectively detect specific field or field gradient components (permitting vector measurements) [Ilmoniemi et al., 1989]. The use of SQUIDs in an unshielded, open environment is complicated by the SQUID's sensitivity to RF interference and mechanical vibrations. As with the magnetic dipole, for RF applications, a tuned circuit is needed to limit the otherwise broad frequency response and reject out-of-band interference.

While sensitivity is a significant advantage of SQUIDs, it can also be a drawback as demonstrated by the LBL experiment. A means of canceling or minimizing significant background noise is essential. One technique is to configure the sensor as a gradiometer where

homogeneous background fields are canceled at the SQUID level. Another technique is to use separate, discrete sensors (as was done in the LBL experiment) and perform the background subtraction at the system level. While both techniques are effective, system level issues must also be considered. The fundamental differences in these two techniques are (i) baseline distance between sense coils, and (ii) dynamic range. In the case of the gradiometer, the baseline distance is quite small. The Conductus HTS sensor is contained in a physically small package and when configured as a gradiometer, it is implemented in a planar arrangement. Small coil separation results in a decreased sensitivity to sources more distant. Therefore to sense a source at a given depth, say > 10 m, coil separation greater than a centimeter is desirable. In order to achieve greater coil separations, the second technique is available; i.e., use two separate, discrete sensors. The challenge of this approach is related to dynamic range. The motivation behind this cancellation is the presence of significant background fields or signals. To measure these background signals independently and then apply a cancellation technique requires that each sensor have a dynamic range covering the background signal level as well as the desired target signal level. This dynamic range may be difficult to achieve.

As with SQUID technology, a gradiometer arrangement may be assembled using magnetic dipoles. Dipole separation may be large (measured in centimeters or meters) and still use a common winding signal on both dipoles. This approach maximizes the dynamic range of the system to that of the dipole and the electronics must accommodate the difference signal only.

In referring to geophysical applications Clarke [1989] points out that while SQUIDs offer a magnetic field resolution of 0.1 $pT/\sqrt{Hz}$ at 1 Hz and 0.01 $pT/\sqrt{Hz}$ at 100 Hz, commercially available coils operated at room temperature offer a resolution of about 0.03 $pT/\sqrt{Hz}$ over this frequency range. So the question to be posed in comparing magnetic dipoles with SQUID technologies for EMI applications is not which is more sensitive, the question is which technology better lends itself to addressing the other systems level problems; namely, size constraints, frequency of interest, and dynamic range.

6.0 List of Symbols

Symbol	Units	Name
A	m^2	average-turns area in coil
A_c	m^2	available winding cross-sectional area
A_f	m^2	ferromagnetic core cross-sectional area
A_w	m^2	single wire cross-sectional area
a	m	average-turns radius
BW	Hz	bandwidth
C	F	coil capacitance
C_T	F	tank circuit capacitance
e.m.f.	V	electromotive force
e_n	$V/\sqrt{Hz}$	equivalent input noise voltage
f	Hz	frequency
H	A/m	magnetic intensity
h	J s	Plank's constant, 6.6256×10^{-34} J s
i_i	A	input current
i_s	A	SQUID current
I_o	A	SQUID critical current
k	J/K	Boltzmann's constant, 1.38×10^{-23} J/K
k_{si}	--	coupling coefficient between input and SQUID circuits
K_e	--	effective relative permeability
K_m	--	true relative permeability
L	H	coil inductance
L_i	H	input coil inductance
L_s	H	SQUID inductance
L_T	H	tank circuit inductance
m	--	length-to-diameter ratio
n	--	number of turns in coil
$N/4\pi$	--	demagnetizing factor
Q	--	quality factor
q	C	electronic charge, 1.60218×10^{-19} C
R	Ω	internal coil resistance
R_{in}	Ω	receiver input resistance
R_T	Ω	tank circuit resistance
$S_v(\omega)$	$V/\sqrt{Hz}$	open-circuit, thermal-noise voltage spectral density
$S_h(\omega)$	$A/m/\sqrt{Hz}$	equivalent magnetic field noise spectral density
T	K	physical temperature
v_r	V	SQUID readout voltage
Z_f	Ω	small-signal forward transfer ratio
Φ_o	Wb	flux quantum, 2.07×10^{-15} Wb
Φ_{si}	Wb	coupled flux
θ_{si}	--	normalized SQUID flux
μ_o	H/m	permeability of free space, $4\pi \times 10^{-7}$ H/m
σ_c	S/m	wire conductivity
ω	radians/s	radian frequency, $2\pi f$
ω_R	radians/s	resonant frequency

7.0 References

Bozorth, R. M., *Ferromagnetism*, IEEE Press, New York, pp. 845-849, 1978.

Burrows, M. L., *ELF Communications Antennas*, Peter Peregrinus Ltd., Stevenage, England, pp. 162-167, 187-207, 1978.

Clarke, J., "Principles and Applications of SQUIDs," *Proceedings of the IEEE*, v. 77(8), pp. 1208-1223, 1989.

Clarke, J., "SQUIDs," *Scientific American*, pp. 46-53, August 1994.

Conductus, Inc. product literature, 1995.

Falco, C. M., "SQUIDs: Applications Outside The Laboratory," *Phys. Technology*, v. 9, pp. 148-153, 1978.

Giffard, R. P., "Fundamentals of SQUID Applications," in *SQUID '80, Superconducting Quantum Interference Devices and their Applications*, H. D. Hahlbohm and H. Lubbig eds., Walter de Gruyter & Co., Berlin, p. 445-471, 1980.

Ilmoniemi, R., J. Knuutila, T. Ryhanen, and H. Seppa, "Multi-SQUID Devices And Their Applications," in *Progress in Low Temperature Physics*, D. F. Brewer, ed., Elsevier Science Publishers, Amsterdam, pp. 271-339, 1989.

Keller, G. V. and F. C. Frischknecht, *Electrical Methods in Geophysical Prospecting*, Pergamon Press, Oxford, England, 1966.

Ragor, D., Los Alamos National Laboratory, personal communication, 9/6/95.

Stolarczyk, L, of RTR, Inc., personal communication, 5/1/95, 6/28/95.

Wilt, M., N. E. Goldstein, M. Stark, J. R. Haught, and H. F. Morrison, "Experience with the EM-60 Electromagnetic System for Geothermal Exploration in Nevada," *Geophysics*, v. 48(8), pp. 1090-1101, 1983.

8.0 Bibliography

8.1 Electromagnetic Induction

Boyd, G. W. and C. J. Wiles, "The Newmont Drill-Hole EMP System-Examples From Eastern Australia," *Geophysics*, v. 49(7), pp. 949-956, 1984.

Corbyn, J. A., "Pulse Induction Metal Detection," *Wireless World*, pp. 40-44, March 1980.

Das, Y., J. E. McFee, and R. H. Chesney, "Determination of Depth of Shallowly Buried Objects by Electromagnetic Induction," *IEEE Transactions on Geoscience and Remote Sensing*, v. 23(1), pp. 60-65, 1985.

Das, Y., J. E. McFee, and R. H. Chesney, "Time Domain Response of a Sphere in the Field of a Coil: Theory and Experiment," *IEEE Transactions on Geoscience and Remote Sensing*, v. 22(4), pp. 360-367, 1984.

Das, Y., J. E. McFee, J. Towes, and G. C. Stuart, "Analysis of an Electromagnetic Induction Detector For Real-Time Location of Buried Objects," *IEEE Transactions Geoscience and Remote Sensing*, v. 28(3), pp. 278-287, 1990.

Das, Y. and J. E. McFee, "A Simple Analysis of The Electromagnetic Response of Buried Conducting Objects," *IEEE Transactions on Geoscience and Remote Sensing*, v. 29(2), pp. 342-344, 1991.

Dyck, A. V. and G. F. West, "The Role of Simple Computer Models in Interpretations of Wide-Band, Drill-Hole Electromagnetic Surveys in Mineral Exploration," *Geophysics*, v. 49(7), pp. 957-980, 1984.

Hill, D. A. and K. H. Cavcey, "Coupling Between Two Antennas Separated by a Planar Interface," *IEEE Transactions on Geoscience and Remote Sensing*, v. 25(4) pp. 422-431, 1987.

Lee, T., "The Transient Electromagnetic Response of a Conducting Sphere in an Imperfectly Conducting Half-Space," *Geophysical Prospecting*, v. 31, pp. 766-781, 1983.

McCracken, K. G., M. L. Oristaglio, and G. W. Hohmann, "Minimization of Noise in Electromagnetic Exploration Systems," *Geophysics*, v. 51(3), pp. 819-832, 1986.

McFee, J. E. and Y. Das, "The Detection of Buried Explosive Objects," *Canadian Journal of Remote Sensing*, v. 6, pp. 104-121, 1980.

Moffatt, D. L. and R. J. Puskar, "A Subsurface Electromagnetic Pulse Radar," *Geophysics*, v. 41(3), pp. 508-518, 1976.

Schneider, J., J. Brew, and I. C. Peden, "Electromagnetic Detection of Buried Dielectric Targets," *IEEE Transactions on Geoscience and Remote Sensing*, v. 29(4), pp. 555-562, 1991.

Sebak, A. A. and L. Shafai, "Transient Response Computation of Spheroidal Objects Using Impedance Boundary Conditions," *IEEE Transactions on Antennas and Propagation*, v. 32(4), 1984.

Stolarczyk, L G., "Radio Imaging in Seam Waveguides," *Geotechnical and Environmental Geophysics*, v. 3, Investigations in Geophysics, 5(3), pp. 187-209, 1991.

Stolarczyk, L, of RTR, Inc., personal communication, 5/1/95, 6/28/95.

Wilt, M., N. E. Goldstein, M. Stark, J. R. Haught, and H. F. Morrison, "Experience with the EM-60 Electromagnetic System for Geothermal Exploration in Nevada," *Geophysics*, v. 48(8), pp. 1090-1101, 1983.

8.2 Airborne Electromagnetic Induction Techniques

Annan, A. P., "Development of The PROSPECT I Airborne Electromagnetic System;" in Palacky, G. J., ed., *Airborne Resistivity Mapping,* Geological Survey of Canada, Ottawa, Paper 86-22, pp. 63-70, 1986.

Barnett, C. T., "Simple Inversion of Time-Domain Electromagnetic Data," *Geophysics*, v. 49(7), pp. 925-933, 1984.

Best, M. E. and T. G. T. Bremner, "The Sweepem Airborne Electromagnetic System," in Palacky, G. J., ed., *Airborne Resistivity Mapping,* Geological Survey of Canada, Ottawa, Paper 86-22, pp. 71-77, 1986.

Collett, L. S., "Development of The Airborne Electromagnetic Technique," in Palacky, G. J., ed., *Airborne Resistivity Mapping,* Geological Survey of Canada, Ottawa, Paper 86-22, pp. 9-18, 1986.

Frasier, D. C. "A New Multicoil Aerial Electromagnetic Prospecting System," *Geophysics*, v. 37(3), pp. 518-537, 1972.

Fraser, D. C., "Dighem Resistivity Techniques in Airborne Electromagnetic Mapping," in Palacky, G. J., ed., *Airborne Resistivity Mapping,* Geological Survey of Canada, Ottawa, Paper 86-22, pp. 49-54, 1986.

Herz, A., "Airborne EM Instruments Operating at VLF And Higher Frequencies," in Palacky, G. J., ed., *Airborne Resistivity Mapping,* Geological Survey of Canada, Ottawa, Paper 86-22, pp. 55-61, 1986.

Hogg, R. L. S, "The Aerodat Multigeometry, Broadband Transient Helicopter Electromagnetic System," in Palacky, G. J., ed., *Airborne Resistivity Mapping,* Geological Survey of Canada, Ottawa, Paper 86-22, pp. 79-89, 1986.

Holladay, J. S, N. Valleau, and E. Morrison, "Application of Multifrequency Helicopter Electromagnetic Surveys to Mapping of Sea-Ice Thickness and Shallow-Water Bathymetry," in Palacky, G. J., ed., *Airborne Resistivity Mapping,* Geological Survey of Canada, Ottawa, Paper 86-22, pp. 91-98, 1986.

Macnae, J. C., R. Smith, B. D. Polzer, Y. Lamontagne, and P. S. Klinkert, "Conductivity-Depth Imaging of Airborne Electromagnetic Step-Response Data," *Geophysics*, v. 56(1), pp. 102-114, 1991.

Palacky, G. J., "Geological Background to Resistivity Mapping," in Palacky, G. J., ed., *Airborne Resistivity Mapping,* Geological Survey of Canada, Ottawa, Paper 86-22, pp. 19-27, 1986.

Paterson, N. R. and S. W. Reford, "Inversion of Airborne Electromagnetic Data for Overburden Mapping And Groundwater Exploration," in Palacky, G. J., ed., *Airborne Resistivity Mapping,* Geological Survey of Canada, Ottawa, Paper 86-22, pp. 38-48, 1986.

Smith, R. S. and P. B. Keating, "The Utility of Multicomponent Time-Domain Electromagnetic Measurements," product literature from GEOTERREX, Inc., 1994.

West, G. F., "Modeling of Airborne Electromagnetic Response: Present Capabilities and Future Expectations," in Palacky, G. J., ed., *Airborne Resistivity Mapping,* Geological Survey of Canada, Ottawa, Paper 86-22, pp.29-38, 1986.

8.3 Magnetic Dipole Antennas

Bozorth, R. M., *Ferromagnetism*, IEEE Press, New York, pp. 845-849, 1978.

Burrows, M. L., *ELF Communications Antennas*, Peter Peregrinus Ltd., Stevenage, England, pp. 162-167, 187-203, 1978.

Hill, D. A. and J. R. Wait, "Coupling Between a Dipole Antenna And an Infinite Cable Over an Ideal Ground Plane," *Radio Science*, v. 12(2), pp. 231-238, 1977.

Hill, D. A., "Magnetic Dipole Excitation of a Long Conductor in a Lossy Medium," *IEEE Transactions on Geoscience and Remote Sensing*, v. 26(6), pp. 720-725, 1988.

Hill, D. A., "Magnetic Dipole Excitation of an Insulated Conductor of Finite Length," *IEEE Transactions on Geoscience and Remote Sensing*, v. 28(3), pp. 289-294, 1990.

Keller, G. V. and F. C. Frischknecht, *Electrical Methods in Geophysical Prospecting*, Pergamon Press, Oxford, England, 1966.

King R., W. P. and K. Iizuka, "The Complete Electromagnetic Field of a Half-Wave Dipole in a Dissipative Medium," *IEEE Transactions on Antennas and Propagation*, v. AP-11, pp. 275-285, 1963.

Peden, I. C., R. Kipp, and J. Allestad, "A Scale-Model Study of Down-Hole VHF Dipole Arrays with Application to Subsurface Exploration," *IEEE Transactions Geoscience. and Remote Sensing*, v. 30(5), pp. 885-891, 1992.

Sivaprasad, K. and R. W. P. King, "A Study of Arrays of Dipoles in a Simi-Infinite Dissipative Medium," *IEEE Transactions on Antennas and Propagation*, v. AP-11, pp. 240-256, 1963.

Wait, J. R., "The Receiving Loop with a Hollow Prolate Spherical Core," *Canadian Journal of Technology*, v. 31, pp. 132-137, 1953.

Wait, J. R., "Insulated Loop Antenna Immersed in a Conducting Medium," *Journal of Research of the National Bureau of Standards*, v. 59(2), pp. 133-137, 1957.

Wu, T. T., R. W. P. King, and D. V. Giri, "The Insulated Dipole Antenna in a Relatively Dense Medium," *Radio Science*, v. 8(7), pp. 699-709, 1973.

8.4 SQUID Technology

Barone, A. *Principles And Applications of Superconducting Quantum Interference Devices*, World Scientific Publishing Co., Singapore, 1992.

Burrows, M. L., *ELF Communications Antennas*, Peter Peregirnus Ltd., Stevenage, England, pp. 203-207, 1978.

Clarke, J., "Principles and Applications of SQUIDs," *Proceedings of the IEEE*, v. 77(8), pp. 1208-1223, 1989.

Clarke, J., "SQUIDs," *Scientific American*, pp. 46-53, August 1994.

Conductus, Inc. product literature, 1995.

Danilov, V. V., K. K. Likharev, and O. V. Snigirev, "Signal and Noise Parameters of SQUIDs," in *SQUID '80, Superconducting Quantum Interference Devices and their Applications*, H. D. Hahlbohm and H. Lubbig, eds., Walter de Gruyter & Co., Berlin, pp. 473-507, 1980.

Falco, C. M., "SQUIDs: Applications Outside The Laboratory," *Phys. Technology*, v. 9, pp. 148-153, 1978.

Feynman, R. P., R. B. Leighton, and M. Sands, *The Feynman Lectures on Physics*, Addison-Wesley, Reading, Massachusetts, v. 3, chapter 21, pp. 14-18, 1965.

Giffard, R. P., "Fundamentals of SQUID Applications," in *SQUID '80, Superconducting Quantum Interference Devices and their Applications*, H. D. Hahlbohm and H. Lubbig eds., Walter de Gruyter & Co., Berlin, p. 445-471, 1980.

Ilmoniemi, R., J. Knuutila, T. Ryhanen, and H. Seppa, "Multi-SQUID Devices And Their Applications," in *Progress in Low Temperature Physics*, D. F. Brewer, ed., Elsevier Science Publishers, Amsterdam, pp. 271-339, 1989.

Jackson, T. J., M. N. Keene, and C. E. Gough, "A SQUID Magnetometer For Low Field DC Magnetization And AC Susceptibility Measurements," *Meas. Sci. Technology*, v. 3, pp. 988-991, 1992.

Reagor, D., Los Alamos National Laboratory, personal communication, 9/6/95.

Wilt, M., N. E. Goldstein, M. Stark, J. R. Haught, and H. F. Morrison, "Experience with the EM-60 Electromagnetic System for Geothermal Exploration in Nevada," *Geophysics*, v. 48(8), pp. 1090-1101, 1983.